Journal of Applied Electrochemistry **33**: 205–215, 2003.

Study of mass transfer in a vertically moving particle bed electrode

K. BOUZEK[1,*], R. CHMELÍKOVÁ[2], M. PAIDAR[1] and H. BERGMANN[3]
[1]*Department of Inorganic Technology, Institute of Chemical Technology, Technická 5, 166 28 Prague 6, Czech Republic*
[2]*Department of Chemical Engineering, Institute of Chemical Technology, Technická 5, 166 28 Prague 6, Czech Republic*
[3]*Anhalt University of Applied Sciences, Bernburger Strasse 55, D-06366 Koethen, Germany*
*(*author for correspondence, e-mail: bouzekk@vscht.cz)*

Received 26 November 2001; accepted in revised form 25 October 2002

Key words: electrochemical reactor, mass transfer, metal removal, rotating drum, three-dimensional electrode

Abstract

A study was made of the influence of process parameters on the mass-transfer coefficient in a flow-through cell with a cascade of rotating drums partially filled with conductive particles (called the 'vertically moving particle bed'). Copper deposition from an acidic sodium sulphate solution was used as the model reaction. To evaluate the experimental data a macrohomogeneous mathematical model of potential and current density distribution inside the cell was developed. The electrolyte flow distribution between the empty space above the particle bed and through the bed was evaluated. On the basis of these results the following correlation is proposed:

$$Sh = \frac{1.09}{\varepsilon} Re_p^{1/3} Sc^{1/3} + \frac{52.8\, Re_r}{2498 + Re_r}\{1 - \exp[-125(1.04 \times 10^{-6} Re_r + Re_p)]\}$$

where the first term corresponds to the packed bed electrode and the second term represents the contribution of bed rotation. It is valid for bed porosity of 45%, cathode drum rotation rates between 0.047 and 0.120 Hz (i.e., 2.8 to 7.2 rpm) and a Re_p range of 0.003 to 0.013.

List of symbols

a	constant (Equation 24)
A	specific surface (m^{-1})
c	molar concentration (mol m^{-3})
C	capacity (F)
d	diameter (m)
D	diffusion coefficient (m^2 s^{-1})
e_{dis}	dissipative energy (m^2 s^{-2})
E	electrode potential (V)
f	frequency of drum rotation (s^{-1})
F	faradaic constant (C mol^{-1})
g	gravitational acceleration (m s^{-2})
h	electrode height (m)
j	current density (A m^{-2})
j_0	exchange current density (A m^{-2})
j_D	Chilton–Colburn factor, $j_D = \frac{k}{v} Sc^{2/3}$
J	copper depletion rate (mol s^{-1})
k	mass transfer coefficient (m s^{-1})
L	length (distance) (m)
n	number of moles (mol)
p	pressure (Pa)
q	charge (C)
r	radius (m)
R	universal gas constant (J K^{-1} mol^{-1})
Re_c	Reynolds number of convective flow, $Re_c = \dot{V}/h\varepsilon v$
Re_p	Reynolds number for packed bed cathode, $Re_p = d_p v/v$
Re_r	Reynolds number for drum rotation, $Re_r = f d_d^2/v$
$Re_{r,B}$	Reynolds number for packed bed rotation, $Re_{r,B} = \omega r_2^2/v$
Sc	Schmidt number, $Sc = v/D$
Sh	Sherwood number, $Sh = kd/D$
S	area (m^2)
t	tortuosity factor
T	temperature (K)
U	cell voltage (V)
v	superficial velocity (m s^{-1})
V	volume (m^3)
$\dot{V}$	volumetric flow rate (m^3 s^{-1})
x	coordinate (m)
z	ion charge number

Greek symbols

α	charge transfer coefficient
β	constant (Equation 1)
ε	bed porosity

η overvoltage (V)
η_S dynamic viscosity of the electrolyte (Pa s)
φ Galvani potential (V)
κ conductivity (S m^{-1})
ν kinematic viscosity (m^2 s^{-1})
ρ resistivity (Ω m)
$\bar{\rho}$ density (kg m^{-3})
τ time (s)
ω angular rotation rate (s^{-1})
Ψ constant (Equation 34)

Subscripts
a anode
an anode compartment
ch channel
Cu with respect to copper
H with respect to hydrogen
i number of the drum
int four cathode drums facing an anode on each side
l left-hand side
lim limiting
L reactor outlet, reservoir inlet
m metal
r right-hand side
s solution
sep separator
p particle
pb packed bed
R reservoir
x position
0 reactor inlet, reservoir outlet

Superscripts
m metal
s solution
0 reactor inlet

1. Introduction

The application of three-dimensional (3D) electrodes represents the most widespread electrochemical method of removing heavy metal ions from dilute solutions. This is mainly because of the high mass transfer rate and high specific surface of 3D electrodes.

Several types of 3D electrode have been proposed, for example, carbon or metal particles [1, 2], metallic or metal plated foams and felts [3, 4] and reticulated vitreous carbon [2]. Metallic or carbon felt electrodes have been identified as the most suitable [5], mainly because of their high specific surface area and high mass transfer rates between the liquid phase and the electrode surface. Furthermore, graphite felt has good stability, electrical conductivity and high overvoltage for the hydrogen evolution reaction. The main drawback of these electrodes, however, is the fact that continuous metal deposition leads to clogging of the pores by the deposited metal. Packed bed electrodes consisting of metal particles represent a cheaper alternative to felt electrodes. Here the agglomeration of individual particles poses a similar problem. Both these effects lead to decreased specific surface area and increased hydraulic resistance of the electrode. This results in the need to stop the process at regular intervals in order either to change or regenerate the cathode.

One possibility of avoiding the problem of clogging or agglomeration is the use of a fluidised 3D electrode [2]. A rotating cathode drum filled with conductive particles combines the advantages of packed and fluidising bed electrodes. Rotation of the 3D electrode prevents particle agglomeration. Slow rotation, on the other hand, maintains electronic contact between the particles equivalent to that of the packed bed cathode. Initially the advantages of this arrangement were recognised with respect to the galvanization of small items [6]. Its application to wastewater treatment was proposed later [7–9]. More recently a new type of cell characterised by a high filling degree of the drum was proposed [10]. Different variants of this cell have been constructed [11]. A recent one includes several drums on a common rotation shaft, forming a cascade of reactors. Given a suitable construction, self-classification of the electrode particles according to size and automatic removal of the largest particles are possible. This type of reactor is called a 'vertically moving particle bed' (VMPB) cell.

Mass transfer is a crucial factor with regard to process efficiency in the electrochemical treatment of dilute solutions and it has generated numerous studies. Authors have focused on felt [12–15], reticulated electrodes [3, 16, 17] and fluidised electrodes [18].

Studies published before 1978 on the problem of mass transfer in particulate packed bed electrodes were reviewed by Newman and Tiedemann [19]. Further publications on this problem followed [20–24]. The general form of dimensionless criteria, Equation 1, is predominantly used to describe the experimental data [20–22, 25–27].

$$Sh = \beta_1 Re_p^{\beta_2} Sc^{1/3} \quad (1)$$

Particle diameter is used as a characteristic dimension. The values of the coefficients β_1 and β_2, obtained by different authors, together with the limits of validity are given in Table 1.

Table 1. Published parameters for the correlation equation $Sh = \beta_1 Re^{\beta_2} Sc^{1/3}$

Source	Range of validity	β_1	β_2
20	$0 < Re_p < 45$	2.277	1/3
21	$0.05 < Re_p < 30$	4.58	1/3
22	$10 < Re_p < 145$	1.46	0.72
25	$0.0016 < Re_p < 55$	$1.09/\varepsilon$	1/3
26	$50 < Re_p < 5000$	0.5	0.61
27	$100 < Re_p < 10\,000$	0.32	0.66

Some authors modified this equation to improve its accuracy [23, 28, 29]. An alternative means of mass transfer correlation in a packed bed electrode is given by the Chilton–Colburn factor, j_D [24]:

$$j_D = 2.944\ Re_p^{-0.554}\left(\frac{L}{d_p}\right)^{-0.15} \tag{2}$$

The advantages of rotating packed bed cathodes were acknowledged by Kreysa [30] who discusses the mass-transfer correlation of Brandner [31]:

$$Sh = 0.454 \times Sc^{1/3}\left[Re_c^2 + \left(Re_{r,B}\frac{d_e}{\varepsilon r_2}\right)^2\right]^{0.290}\left(\frac{d_e}{r_2 - r_1}\right)^{1.116} \tag{3}$$

where r_1 and r_2 are the inner and outer diameters of the rotating packed bed, Re_c the Reynolds number for the convective flow and $Re_{r,B}$ the Reynolds number for the bed rotation rate. The main advantage of this arrangement is that it allows control of the mass transfer coefficient value independent of electrolyte flow rate, that is, residence time inside the cell.

Apart from a range of papers on the problem of packed bed electrodes, no publication on the VMPB cell has appeared to date. The only study published on the problem of mass transfer in a rotating packed bed electrode is by Kreysa [30] who deals with a differently constructed system and electrolyte hydrodynamics. These results are not, therefore, applicable to the VMPB. The aim of the present work is to determine the influence of electrolyte flow and electrode rotation rate on the mass transfer coefficient in a pilot plant-scale VMPB cell and thus to fill this gap.

2. Mathematical model

The mass balance in a plug flow reactor working under limiting current conditions can be expressed by

$$-\frac{\partial c_x}{\partial \tau} = \frac{\dot{V}}{S}\frac{\partial c_x}{\partial x} + kAc_x \tag{4}$$

A plug flow reactor model was chosen because the mathematical treatment is simpler. The cell construction and experimental arrangement are given below in the experimental part of the work. For an ideally mixed reservoir the following mass balance can be expressed by

$$\dot{V}c_L - \dot{V}c_0 = V_R\frac{dc_0}{d\tau} \tag{5}$$

Equations 4 and 5 have to be solved. In the present work the assumption was made that in comparison to the reservoir the volume of the reactor is negligible, which means that for the period that the electrolyte passes through the cell the inlet concentration may be considered to remain constant, that is, $dc_x/d\tau = 0$. Given this assumption, Equation 4 can be solved analytically:

$$c_L = c_0 \exp\left(-\frac{Ak}{v}L\right) \tag{6}$$

The mass transfer coefficient k can now be expressed by the copper depletion rate J.

$$k = -\frac{\dot{V}}{ASL}\ln\left(1 + \frac{J}{\dot{V}c_0}\right) \tag{7}$$

where J may be expressed either on the basis of the concentration change during the single passage of the electrolyte through the cell, Equation 8, or the concentration change in the reservoir, Equation 9:

$$J = \dot{V} \times (c_L - c_0) \tag{8}$$

$$J = \frac{dc_0}{d\tau} \times V_R \tag{9}$$

As mentioned above, Equation 7 is only valid for fully mass transfer controlled processes.

A one-dimensional macrohomogeneous model of the cell was developed to verify the validity of the assumption of uniform electrode activity across the drum and to evaluate the mass transfer coefficient values. Two parallel electrical current pathways were considered: (i) the cathode particles and (ii) the electrolyte. The potential drop in each continuum was calculated using Equations 10 and 11, respectively:

$$\kappa^m\frac{d^2\varphi^m}{dx^2} = -j_{el,x} \times A \tag{10}$$

$$\kappa^s\frac{d^2\varphi^s}{dx^2} = j_{el,x} \times A \tag{11}$$

The value of $j_{el,x}$, corresponds to the current density related to the cathode reactions. Copper deposition and hydrogen evolution were considered to take place on the cathode surface. The total current density is given by the sum of the two partial values:

$$j_{el,x} = j_{Cu,x} + j_{H,x} \tag{12}$$

The oxygen reduction reaction was neglected. This is due mainly to the fact that the diaphragm separates the anode and cathode compartments. The oxygen evolved can thus only penetrate to the cathode at a limited rate. This was supported by indirect evidence. Experimentally it was demonstrated that in the absence of the separator the copper concentration in the solution does not decrease below 0.16 mol m^{-3} (i.e., 10 mg dm^{-3}). This was due to copper redissolution. If the separator is present, copper concentration lower than 0.01 mol m^{-3} was attained reproducibly under the test conditions. This clearly documents the decelerating effect of the

separator on oxygen transfer to the cathode compartment. In the present work the concentration decay was studied down to a value of 0.16 mol m^{-3}, that is, its concentration was much higher than that of oxygen. Moreover, the material balance of Cu^{2+} was used to determine the mass transfer coefficient. The influence of oxygen reduction on its value can therefore be neglected provided that the bed is working in a mass transfer limited regime. Individual current densities were evaluated by means of the following polarization curves.

$$j_{\mathrm{Cu},x} = \frac{-j_{0,\mathrm{Cu},x}\left[\exp\left(-\frac{\alpha_{\mathrm{Cu},c} z_{\mathrm{Cu}} F}{RT}\eta_{\mathrm{Cu},x}\right) - \exp\left(\frac{(1-\alpha_{\mathrm{Cu},c}) z_{\mathrm{Cu}} F}{RT}\eta_{\mathrm{Cu},x}\right)\right]}{1 - \frac{j_{0,\mathrm{Cu},x}}{j_{\mathrm{lim,Cu},x}}\exp\left(-\frac{\alpha_{\mathrm{Cu},c} z_{\mathrm{Cu}} F}{RT}\eta_{\mathrm{Cu},x}\right)} \tag{13}$$

$$j_{\mathrm{H},x} = -j_{0,\mathrm{H}}\exp\left(-\frac{\alpha_{\mathrm{H},c} z_{\mathrm{H}} F}{RT}\eta_{\mathrm{H},x}\right) \tag{14}$$

The following values of the required kinetic parameters were established experimentally [32]: $j_{0,\mathrm{Cu}} = 1.026\ c_{\mathrm{Cu}}$, $j_{0,\mathrm{H}} = 1.26 \times 10^{-3}$ A m^{-2}, $\alpha_{\mathrm{Cu},c} = 0.40$ and $\alpha_{\mathrm{H},c} = 0.57$. The reversible potential of individual electrode reactions was obtained using the Nernst equation. Standard redox potentials of $E^{\circ}_{\mathrm{Cu^{2+}/Cu}} = 0.337$ V and $E^{\circ}_{\mathrm{H^{+}/0.5H_2}} = 0.0$ vs NHE were considered in [32]. The limiting current density of Cu deposition $j_{\mathrm{lim,Cu}}$ was calculated using Equation 15.

$$j_{\mathrm{lim,Cu},x} = -kAc_{\mathrm{Cu},x}zF \tag{15}$$

The local value of the Cu^{2+} concentration was derived by integrating Equation 16.

$$\frac{\mathrm{d}c_{\mathrm{Cu}}}{\mathrm{d}x} = \frac{j_{\mathrm{Cu},x}A}{z_{\mathrm{Cu}}Fv} \tag{16}$$

The current density value on the separator (identical to the anodic current density) was obtained by integrating the local current density values according to Equation 17.

$$\frac{\mathrm{d}j_{\mathrm{a}}}{\mathrm{d}x} = -j_{\mathrm{el},x}A \tag{17}$$

Oxygen evolution was the only reaction considered to take place on the anode surface. The potential value of the anode was calculated by means of the Tafel equation with the following experimentally determined parameters.

$$E_{\mathrm{a}} = 1.41 + 0.1055 \times \ln j_{\mathrm{a}} \tag{18}$$

The conductivity of the electrolyte in the volume of the 3D electrode was established using the Bruggemann [33] equation:

$$\overline{\rho}_{\mathrm{s}} = \rho_{\mathrm{s}} \times \left(1 + 1.5\frac{V_{\mathrm{m}}}{V_{\mathrm{s}}}\right) \tag{19}$$

The conductivity of the Cu particle electrode was evaluated using the theory of Bockris and Kim [34]. According to this theory each particle is subject to two forces, a gravitational and an electrostatic force. The electrostatic force can be neglected for the size of the particles used in the present study. The following input parameters were used: a value of 3 for a constant describing particle shape [34], an elastic limit of 0.005 [34], Young's modulus of elasticity 1.2×10^{11} Pa [35] and Cu conductivity of 5.88×10^{7} S m^{-1} [35]. For the surface oxide film conductivity of 4×10^{4} S m^{-1} and thickness of 2×10^{-9} m was used. With these parameters the conductivity of the layer of Cu particles (0.1 m height, $d_{\mathrm{p}} = 2 \times 10^{-3}$ m) was calculated to be $\kappa^{\mathrm{m}} = 9800$ S m^{-1}.

The cathode current feeder passes through the whole depth of the first cathode drum (see Figures 1 and 2). A constant potential of cathode particles φ^{m} was assumed here. Equation 10 has not, therefore, to be solved for the first drum. Boundary conditions expressed by

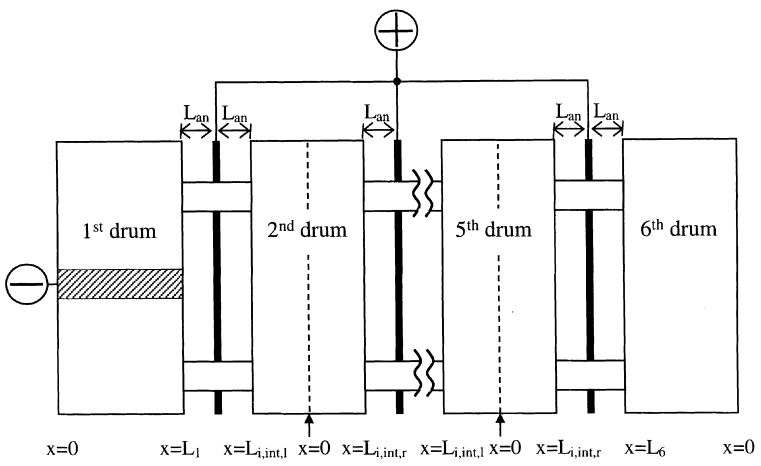

Fig. 1. Simplified scheme of the VMPB cell; the main dimensions used in the mathematical model are indicated.

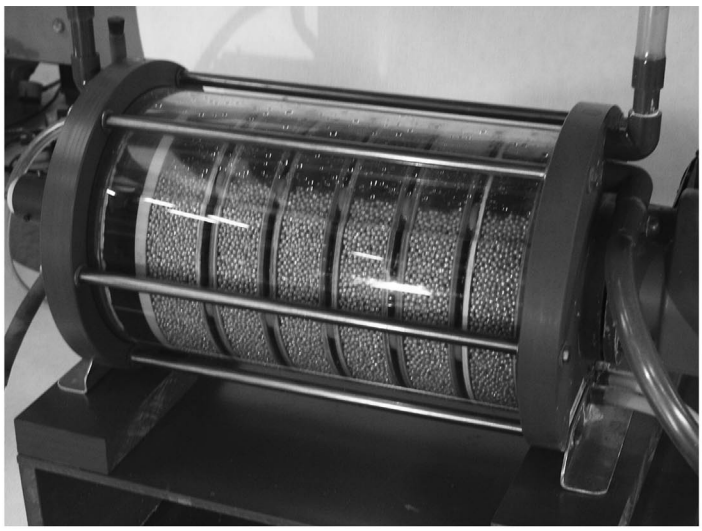

(a)

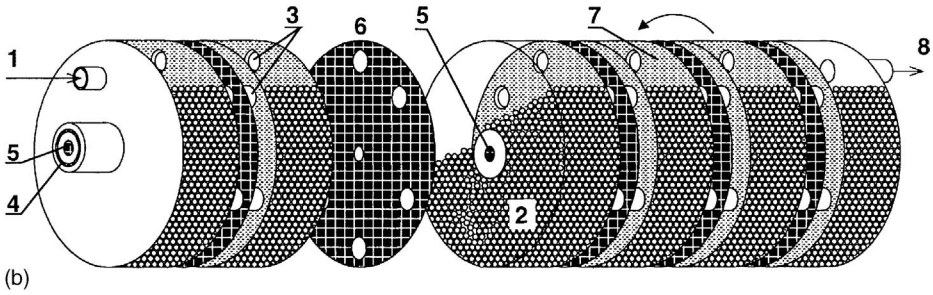

Fig. 2. (a) Overall view of the VMPB cell used during the experiments; (b) Schematic sketch of the arrangement of the drums, anodes, channels and separators inside the VMPB cell: (1) electrolyte inlet, (2) particle bed, (3) channels between individual drums, (4) cathode current feeder, (5) anode current feeder, (6) anode, (7) separator and (8) electrolyte outlet.

Equation 20(a,b) were used to integrate Equation 11, Equation 20(c) to integrate Equation 16 and Equation 20(d) to integrate the current density on the separator, Equation 17:

$$x = 0 \quad \frac{\mathrm{d}\varphi^{\mathrm{s}}}{\mathrm{d}x} = 0 \tag{20a}$$

$$x = L_1 \quad \varphi^{\mathrm{s}} = U_{\mathrm{cell}} - E_{\mathrm{a}} - \frac{j_{\mathrm{a}}}{\kappa^{\mathrm{s}}} \times L_{\mathrm{an}} - t \times \frac{j_{\mathrm{a}}}{\kappa^{\mathrm{s}}} \times L_{\mathrm{sep}} \tag{20b}$$

$$x = 0 \quad c_{\mathrm{Cu}^{2+}} = c^{0}_{\mathrm{Cu}^{2+}} \tag{20c}$$

$$x = 0 \quad j_{\mathrm{a}} = 0 \tag{20d}$$

The positions of individual boundaries are given in a schematic sketch of the cell, see Figure 1. The third and fourth terms in Equation 20(b) correspond to the ohmic drop across the anolyte solution and the separator, respectively.

The remaining drums (2 to 6) have electronic contact to the cathode current feeder only through the particles filling the channels. It is, therefore, also necessary to solve Equation 10. Since anodes are located on each side of drums 2 to 5, the drums have to be split into two regions, each closing the electrical circuit with just one anode. For Equation 10 boundary conditions expressed by Equation 21(a,b) were used. Equation 11 was integrated using the boundary conditions expressed by Equation 21(c,d). Equation 21(e,f) were used to integrate Equations 16 and 17, respectively:

$$x = L_{\mathrm{i,int,l}} \quad \varphi^{\mathrm{m}} = \varphi^{\mathrm{m}}_{\mathrm{L(i-1,int,r)}} + \Delta\varphi_{\mathrm{ch}} \tag{21a}$$

$$x = L_{\mathrm{i,int,l}} \quad \frac{\mathrm{d}\varphi^{\mathrm{m}}}{\mathrm{d}x} = -\frac{\mathrm{d}\varphi^{\mathrm{m}}_{\mathrm{L(i-1,int,r)}}}{\mathrm{d}x} \tag{21b}$$

$$x = 0 \quad \frac{\mathrm{d}\varphi^{\mathrm{s}}}{\mathrm{d}x} = 0 \tag{21c}$$

$$x = L_{\mathrm{i,int,l}} \quad \varphi^{\mathrm{s}} = U_{\mathrm{cell}} - E_{\mathrm{a}} - \frac{j_{\mathrm{a}}}{\kappa^{\mathrm{s}}} \times L_{\mathrm{an}} - t \times \frac{j_{\mathrm{a}}}{\kappa^{\mathrm{s}}} \times L_{\mathrm{sep}} \tag{21d}$$

$$x = L_{\mathrm{i,int,l}} \quad c_{\mathrm{Cu}^{2+}} = c_{\mathrm{Cu}^{2+},L\mathrm{(i-1,int,r)}} \tag{21e}$$

$$x = 0 \quad j_{\mathrm{a}} = 0 \tag{21f}$$

For the right-hand part of these drums the following boundary conditions were applied to solve differential Equations 10, 11, 16 and 17:

$$x = 0 \qquad \varphi^{m}_{i,l} = \varphi^{m}_{i,r} \tag{22a}$$

$$x = 0 \qquad \frac{d\varphi^{m}_{i,l}}{dx} = -\frac{d\varphi^{m}_{i,r}}{dx} \tag{22b}$$

$$x = 0 \qquad \frac{d\varphi^{s}}{dx} = 0 \tag{22c}$$

$$x = L_{i,int,r} \quad \varphi^{s} = U_{cell} - E_a - \frac{j_a}{\kappa^{s}} \times L_{an} - t \times \frac{j_a}{\kappa^{s}} \times L_{sep} \tag{22d}$$

$$x = 0 \qquad c_{Cu^{2+},i,l} = c_{Cu^{2+},i,r} \tag{22e}$$

$$x = 0 \qquad j_a = 0 \tag{22f}$$

The position of $x = 0$ was optimized with respect to the conditions given by Equation 22(d).

The sixth drum, the last, is again associated with only one anode. The following boundary conditions apply here in identical order to the previous ones:

$$x = L_6 \quad \varphi^{m} = \varphi^{m}_{L(5,int,r)} + \Delta\varphi_{ch} \tag{23a}$$

$$x = 0 \quad \frac{d\varphi^{m}_{6}}{dx} = 0 \tag{23b}$$

$$x = 0 \quad \frac{d\varphi^{s}}{dx} = 0 \tag{23c}$$

$$x = L_6 \quad \varphi^{s} = U_{cell} - E_a - \frac{j_a}{\kappa^{s}} \times L_{an} - t \times \frac{j_a}{\kappa^{s}} \times L_{sep} \tag{23d}$$

$$x = L_6 \quad c_{Cu^{2+}} = c_{Cu^{2+},L(5,int,r)} \tag{23e}$$

$$x = 0 \quad j_a = 0 \tag{23f}$$

This set of differential equations was integrated by using the fourth order semi-implicit Runge–Kutta method. The initial conditions were optimized using the modified Newton–Raphson method. The cell voltage corresponding to the current load and mass transfer coefficient value selected was optimized to fit the experimental data using the DNEQNF routine with a modified Powell hybrid algorithm and a finite difference to Jacobian [36].

3. Experimental details

3.1. *Apparatus*

An overall view of the cell used for the experiments is given in Figure 2(a). It consists of 6 rotating drums partially filled with Cu particles with a mean diameter of 2×10^{-3} m. The drums are enclosed in an outer jacket. Five activated titanium anodes are situated between the cathode drums. The cathode particles are separated from the anodes by the PVC diaphragm fixed to the mechanical support on the side walls of the drums. The anodes are connected to the stabilized power supply by the conducting centre of the rotating shaft. The cathode current feeder is located on the rotation shaft in the first cathode drum. Electronic contact to the remaining cathodes is provided through the particles that fill the channels between the individual drums. The channels pass through the holes in the anodes, thus avoiding a short-circuit between the anode and the cathode. The electrolyte enters the cell on the left-hand side and passes through the individual drums. The channels providing contact to the cathode particles between the individual cathode drums also facilitate the electrolyte flow. This prevents the oxygen that has evolved on the anodes from entering the cathode compartment. A schematic sketch of the individual cathode drums, anodes and channels arrangement inside the cell jacket is given in Figure 2(b).

The diameter of the internal drums is 0.165 m, that of the rotation shaft placed in the middle of each drum is 0.060 m. The channels are located on the cell walls approximately 0.010 m away from the circumference of the drums. For this reason during operation a layer of hydrogen up to 0.010 m thick forms on the top of each drum. The diameter of the channels between the drums has a value of 0.016 m. The area of the cross-section of the cathode drum filled with an electrolyte is 1.8×10^{-2} m^2, that filled with cathode particles 1.35×10^{-2} m^2 and the total area of the channels between the individual cathode drums 1.206×10^{-3} m^2. On average, two of the six channels are above the cathode particle level and are thus free of particles. The active area of the channels is 8.04×10^{-4} m^2. The length of each channel is 1.3×10^{-2} m. A PVC diaphragm (Chemische Werke Eilenburg, Germany), 8.0×10^{-4} m thick, is used as a separator between the anode and cathode compartments. A separator tortuosity factor of $t = 25$ was applied during the simulations [32], permitting the calculation of the separator conductivity according to the relationship $\kappa_{sep} = \kappa_s/t$.

The cell was operated in a batch recycle system (i.e., an electrolyte from a reservoir is recycled through the cell). The total volume of the electrolyte was 0.030 m^3. The volume of the electrolyte in the reservoir was 0.024 m^3. The electrolyte flow-rate was controlled by a rotameter. The temperature was kept at 20 °C by a Lauda RM 6S Cryostat.

3.2. *Chemicals*

An electrolyte containing 50 mol H_2SO_4 m^{-3} and 500 mol Na_2SO_4 m^{-3} was used during the experiments. Its conductivity was measured as 4.65 S m^{-1} by a WTW Microprocessor Conductometer LF 2000. The value was independent of the Cu^{2+} concentration in the range studied. The Cu^{2+} diffusion coefficient in the solution was determined to be 5.15×10^{-10} m^2 s^{-1} by a Cu rotating disc electrode. A kinematic viscosity of

1.17×10^{-6} m^2 s^{-1} and density of 1062 kg m^{-3}, given in [35] for 500 mol Na_2SO_4 m^{-3} solution, was selected for the calculations. The initial concentration was 3.2 mol Cu^{2+} m^{-3}, if not otherwise stated. All the chemicals used were of analytical purity grade.

3.3. *Analytical methods*

Samples were taken at regular intervals in the course of electrolysis. The Cu^{2+} content was determined spectrophotometrically at a wavelength of 600 nm. Nanocolor Test 53 (Macherey–Nagel, Germany) was used to form a deep blue complex, thus enhancing analysis accuracy in the low concentration range.

4. Results

The typical course of the Cu^{2+} content in the reservoir against electrolysis time is shown in Figure 3. Two different regions are clearly distinguishable. At the beginning of electrolysis the decrease in Cu^{2+} content in time is linear, later on it changes to exponential decay. Whereas linear concentration decay in the first period is characteristic of the reaction rate controlled by the electrode reaction kinetics, exponential decay indicates a mass transfer controlled process. The Cu^{2+} concentration corresponding to the individual experimental point can be established by dividing the number of moles n by the reservoir volume given in the Figure caption.

For the second electrolysis period the experimental points were fitted by applying an exponential decay curve, see Equation 24. Figure 3 shows the resulting curve together with the experimental data:

$$n = n^0 \exp(-a\tau) \tag{24}$$

From the derivative of this curve, Equation 25, a Cu^{2+} depletion rate, Equation 9, was calculated for each experiment for the series of Cu^{2+} inlet concentrations:

$$J = \frac{dn}{d\tau} = -an^0 \exp(-a\tau) \tag{25}$$

Depletion rates together with the corresponding Cu^{2+} concentrations were applied to calculate mass transfer coefficient values using Equation 7 (plug-flow reactor model) and a macrohomogeneous model of the cell. Mass transfer coefficient values obtained for different electrolyte volumetric flow and cathode drum rotation rates are summarised in Figure 4.

From Figure 4 it follows that the values calculated using the simplified model of the plug flow reactor are almost identical to those using the potential distribution model. This indicates regular current density distribution of Cu deposition along the particle bed electrode. This conclusion was verified by the macrohomogeneous model. As shown in Figure 5, the plug-flow reactor model is fully valid up to a Cu^{2+} inlet concentration of 1.0 mol m^{-3}. Afterwards in the increasing part of the first cathode drum Cu deposition is controlled by the reaction kinetics. This is mainly because the first cathode drum is 0.01 m deeper and at the same time the anode is positioned only on one of its sides. The latter reason also applies in the case of the last drum. Here the Cu deposition starts to be controlled by the electrode reaction kinetics at a Cu^{2+} inlet concentration higher than 2.0 mol m^{-3}. In the case of the first cathode drum the deviation from the plug-flow reactor model is still not very significant with respect to the VMPB cell as a whole. At a Cu^{2+} inlet concentration above 2.0 mol m^{-3} the plug-flow model has only limited validity, because the first and last cathode drums

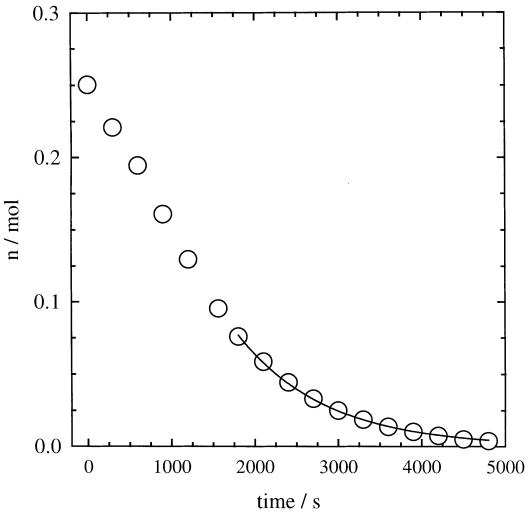

Fig. 3. Dependence of the Cu^{2+} content in the reservoir on the duration of electrolysis. Electrolyte flow rate 5.12×10^{-5} m^3 s^{-1}, current load 25 A, cathode drum rotation rate 0.12 Hz, reservoir volume 2.4×10^{-2} m^3. The curve indicates the least squares fit of the experimental data by Equation 24.

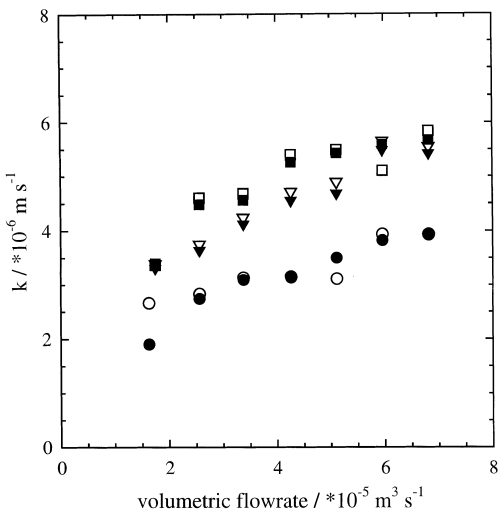

Fig. 4. Dependence of the mass transfer coefficient in the VMPB cell on the electrolyte flow rate. Cathode drum rotation rate: (○) 0.047 Hz, (▽) 0.097 Hz and (□) 0.120 Hz. (Empty symbols) evaluated using plug-flow reactor model, (Filled symbols) evaluated using current density distribution model.

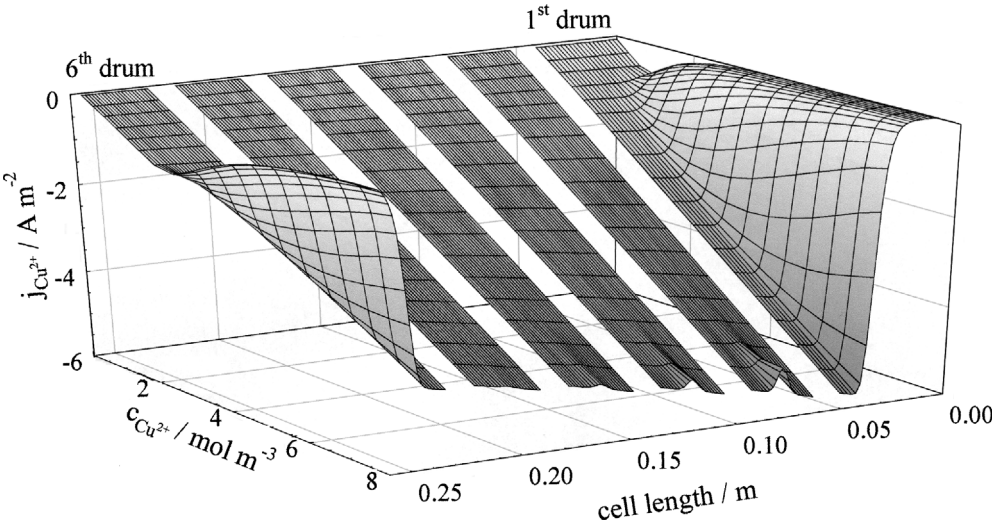

Fig. 5. Simulated dependence of the current density for Cu deposition on the position in the cell and inlet Cu^{2+} concentration; current load 25 A, cathode drum rotation rate 0.047 Hz, electrolyte flow rate 4.27×10^{-5} m^3 s^{-1}.

together already represent an important part of the cell. Above a Cu^{2+} inlet concentration of 6.0 mol m^{-3} the model approximation of the plug-flow reactor is no longer valid. This is because Cu deposition also starts to be controlled kinetically in the central part of the remaining cathode drums. The concentration value at which the process starts to be controlled kinetically is in good agreement with the experimental data. From Figure 3 follows that below a concentration of about 3.0 mol Cu^{2+} dm^{-3} process can be assumed to be mass transfer controlled. This value decreases with decreasing current load and increasing Cu^{2+} flux intensity to the cathode surface. For an evaluation of the mass transfer coefficient typically the Cu^{2+} concentration range below 1.5 mol m^{-3} was studied.

The dependence of the total current density of the electrode reaction j_{el} on the position and the Cu^{2+} inlet concentration is shown in Figure 6. Its course is consistent with the dependence for the Cu deposition reaction shown in the previous figure. Since the cell operates in galvanostatic mode, an enhancement of the current density of the Cu deposition caused by the increasing inlet Cu^{2+} concentration results in a decrease in the current densities of the hydrogen evolution near the separators.

5. Discussion

The mass transfer in the particle bed cathode is controlled by the two parameters (a) electrolyte flow rate and (b) bed rotation. This is consistent with the results shown in Figure 4. The increased contribution of bed rotation and rate is important up to 0.097 Hz. A rise to 0.120 Hz caused only a minor further enhancement of the mass transfer coefficient.

A study of the mass transfer coefficients in the VMPB cell without cathode rotation would cause serious experimental complications because of particle agglomeration. For this reason mass transfer coefficients for a

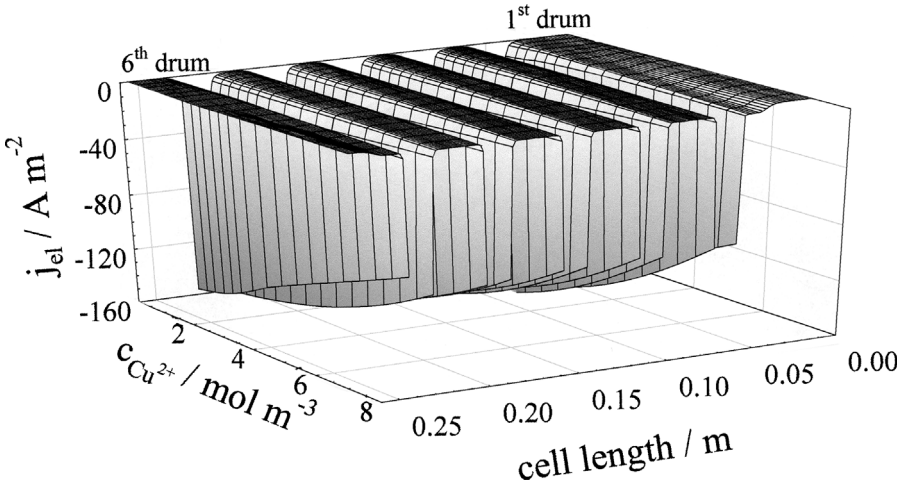

Fig. 6. Simulated dependence of the total current density on the position in the cell and inlet Cu^{2+} concentration; current load 25 A, rotation rate of cathode drum 0.047 Hz, electrolyte flow rate 4.27×10^{-5} m^3 s^{-1}.

packed bed cathode with identical parameters were evaluated using the Sherwood number correlation. This makes it possible to separate the contribution of the bed rotation from the experimental data. In order to evaluate the Reynolds number, the electrolyte flow rate inside the bed has to be evaluated. The reason is that the particles only fill up to 70% of the cross-section of the drums and an important part of the electrolyte passes through the cell by way of the free path above the particles. Equal hydraulic pressure loss along the cathode drum, Equation 26, was assumed:

$$\Delta p_{\text{empty}} = \Delta p_{\text{bed}} \tag{26}$$

The pressure drop along the particle bed was evaluated using the Ergun Equation [37]:

$$\Delta p_{\text{bed}} = \frac{L v_{\text{bed}}}{g d_{\text{p}}} \frac{1-\varepsilon}{\varepsilon^3} \left[\frac{150(1-\varepsilon)\eta_{\text{s}}}{d_{\text{p}}} + 1.75 \bar{\rho}_{\text{s}} v_{\text{bed}} \right] \tag{27}$$

where g is the gravitational acceleration, L the bed length and η_{s} the dynamic viscosity of the electrolyte. The pressure drop in the empty channel was obtained by an expression for the dissipative energy of the laminar flow, Equation 28 [38]:

$$e_{\text{dis}} = \frac{8 \eta_{\text{s}} v_{\text{empty}} L}{\bar{\rho}_{\text{s}} r^2} \tag{28}$$

The bed rotation may disturb the flow laminarity. Since the pressure loss inside the particle bed is clearly higher, in this case the uncertainty introduced by the assumption of laminar flow in the empty channel is not significant. For the horizontal flow and constant channel diameter dissipative energy may also be expressed as follows:

$$e_{\text{dis}} = \frac{\Delta p_{\text{empty}}}{\bar{\rho}_{\text{s}}} \tag{29}$$

Equations 28 and 29 can be combined to obtain:

$$\Delta p_{\text{empty}} = \frac{8 \eta_{\text{s}} v_{\text{empty}} L}{r^2} \tag{30}$$

Superficial electrolyte flow velocities are coupled according to Equation 31.

$$v_{\text{empty}} S_{\text{empty}} + v_{\text{bed}} S_{\text{bed}} = \dot{V} \tag{31}$$

The Ergun Equation 27 and Equation 30 are used to express terms on each side of Equation 26. Equation 31 is used to replace variable v_{empty} by v_{bed}. After rearrangement Equation 32 is obtained:

$$1.75 \frac{\bar{\rho}_{\text{s}}}{g d_{\text{p}}} \frac{1-\varepsilon}{\varepsilon^3} v_{\text{bed}}^2 + \left[\frac{150(1-\varepsilon)^2 \eta_{\text{s}}}{g d_{\text{p}}^2 \varepsilon^3} + \frac{8 \eta_{\text{s}}}{r^2} \frac{S_{\text{bed}}}{S_{\text{empty}}} \right] v_{\text{bed}} - \frac{8 \eta_{\text{s}}}{r^2} \frac{\dot{V}}{S_{\text{empty}}} = 0 \tag{32}$$

This equation can be solved analytically. Parameter r (i.e., the radius of the empty channel) can be obtained by using the relationship for the equivalent diameter d_{e},

$$d_{\text{e}} = \frac{4 S_{\text{empty}}}{L_{\text{c}}} \tag{33}$$

where L_{c} is the circumference of the empty channel.

The superficial electrolyte flow rates inside the bed v_{bed} were evaluated as ranging from 1.78×10^{-6} to 7.45×10^{-6} m s^{-1} for the total volumetric flow rate of the electrolyte 1.63×10^{-5} to 6.82×10^{-5} m^3 s^{-1}. This corresponds to the volumetric flow rate of the electrolyte through the bed (i.e., $\dot{V}_{\text{bed}} = v_{\text{bed}} \times S_{\text{bed}}$) 2.40×10^{-8} to 1.01×10^{-7} m^3 s^{-1}. This means that, without cathode rotation, only 0.15% of the electrolyte flowing through the reactor passes through the particle bed. The remaining portion of the electrolyte passes through the open space above it. This clearly documents a high potential for enhancement of the mass transfer rates inside the cathode bed if the portion of the electrolyte flowing through the bed is increased.

The Re_{p} number inside the cathode varies for the flow rates used in the range of 0.003 to 0.013. Wilson and Geankoplis [25] have proposed a correlation specifically for this Re_{p} range, see Equation 1 and Table 1.

Using the mass transfer enhancement evaluated for the three individual rotation rates as a function of electrolyte flow rate an empirical correlation of the contribution of the bed rotation rate to the Sh number Equation 34 was proposed. Additionally $Sh = Sh_{\text{pb}}$ was assumed for $Re_{\text{r}} = 0$.

$$Sh - Sh_{\text{pb}} = \psi_1 \times \{1 - \exp[\psi_2 \times (\psi_3 Re_{\text{r}} + Re_{\text{p}})]\} \tag{34}$$

where

$$\psi_1 = \frac{52.8 Re_{\text{r}}}{2498 + Re_{\text{r}}} \tag{35}$$

and $\psi_2 = -125$ and $\psi_3 = 1.04 \times 10^{-6}$.

This equation may seem too complex. However, it has to be borne in mind that the problem concerned is significantly more complex when compared with classical correlation functions. Two independent Reynolds numbers which influence the Sherwood number are considered for the packed bed and for the drum rotation. The experimentally determined shape of the dependence exhibits a rise to maximum in both Reynolds numbers. An exponential rise to maximum and rational function were chosen to describe the shape observed for Re_{p} and Re_{r}, respectively. A further serious complication is that the values of Re_{p} and Re_{r} differ by approximately five orders of magnitude. In order to account for both of them and to assure that for the case of $Re_{\text{p}} = 0$ a nonzero value of the Sh number will be obtained, the parameter ψ_3 has to be used. Nevertheless, four parameters (i.e., two for each Reynolds number) do

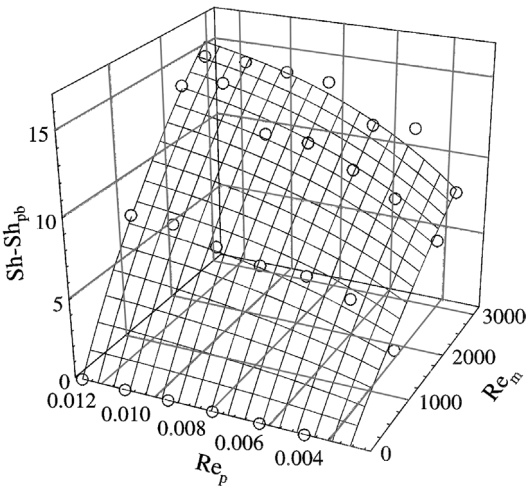

Fig. 7. Dependence of the *Sh* number enhancement by the rotation rate of the cathode drum on the Re_p and Re_r. Circles represent the experimental points; mesh values were calculated using Equation 34.

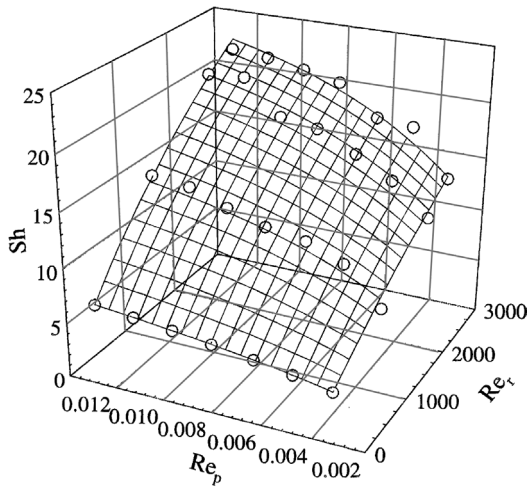

Fig. 9. Dependence of the *Sh* number on Re_p and Re_r. Circles represent the experimental points; mesh values were calculated using Equation 36.

represent an average number used in the majority of correlations. The agreement between the calculated, Equation 34, and the experimentally determined enhancement of the Sherwood number by the cathode rotation is demonstrated in Figure 7. Figure 8 provides the data calculated by using Equation 34 against experimentally determined values, thus permitting a more exact assessment of the agreement of the correlation equation with the experimental data. It conclusively confirms the accuracy of the proposed correlation.

The total mass transfer coefficient depends on both components, that is, mass transfer in the packed bed and enhancement by the bed rotation. For our particular conditions Equation 36 applies:

$$Sh = \frac{1.09}{\varepsilon} Re_p^{1/3} Sc^{1/3} + \frac{52.8\ Re_r}{2498 + Re_r} \times \{1 - \exp[-125 \times (1.04 \times 10^{-6} Re_r + Re_p)]\} \quad (36)$$

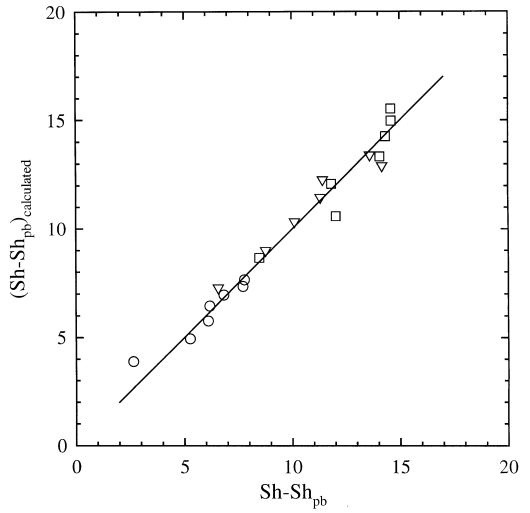

Fig. 8. Comparison of the experimentally determined and calculated contribution of the bed rotation to the *Sh* number, cathode drum rotation rate: (○) 0.047 Hz, (▽) 0.097 Hz and (□) 0.120 Hz.

Agreement with the experimental data is demonstrated in Figure 9. These empirical equation parameters were set for the following experimental conditions: cathode porosity of 45%, Re_r ranging from 0 to 3200 and Re_p from 0.003 to 0.013 (Figure 7). These represent the conditions of interest for the majority of practical applications for this type of cell. Once again it should be emphasized that the Re_p value has to be calculated for the electrolyte flow rate only through the bed.

6. Conclusions

Mass transfer coefficients in the VMPB cathode were determined on the basis of the experimental data using a simplified model of the plug-flow reactor and a complex model that takes into account the current distribution across the individual cathode drums and electrode reaction kinetics. It was found that, in the limited range of the operational parameters, the simplified model of the plug-flow reactor is able to describe the kinetics of the reaction of the electroactive species. This is mainly on account of the regular current density distribution of the copper deposition provided by the cell construction used.

Despite the fact that the cathode drum rotation makes an important contribution (130 to 320% of the value without rotation for the rotation rates used in this study) to the mass transfer value, its total value is lower than that for the packed bed cathode which fills the whole cross-section of the drum. This is because the major part of the electrolyte pumped through the cell passes via an open channel area above the cathode bed. As was evaluated in the present work, it represents approximately 99.8% of the total volumetric flow rate of the electrolyte. This results in a strongly reduced Reynolds number and consequently mass transfer coefficient inside the bed (when compared to the case where 100% of the electrolyte flows through the bed). Bed

rotation only partially eliminates this negative effect. In the present work the contribution of bed rotation was quantified and a suitable empirical correlation of the Sherwood criterion was proposed.

Acknowledgement

The financial support of this research by the Grant Agency of the Czech Republic under project number 104/00/P016 and by the Ministry of Culture Saxony-Anhalt under project number 047A 0821 is gratefully acknowledged. The authors also thank Dr Andreas Rittel (Anhalt University) for practical assistance.

References

1. D.N. Bennion and J. Newman, *J. Appl. Electrochem.* **2** (1972) 113.
2. D. Pletcher and F.C. Walsh, 'Industrial Electrochemistry' (Chapman & Hall, London 1990).
3. A. Tentorio and U. Casolo-Ginelli, *J. Appl. Electrochem.* **8** (1978) 195.
4. A. Montillet, J. Comiti and J. Legrand, *J. Appl. Electrochem.* **23** (1993) 1045.
5. T.L. Hatfield, T.L. Kleven and D.T. Pierce, *J. Appl. Electrochem.* **26** (1996) 567.
6. H. Henig, *DE 21 01 332* (1977).
7. E. Avci, *J. Appl. Electrochem.* **18** (1988) 288.
8. D. Schab and K. Hein, *Metall.* **44** (1990) 362.
9. D. Schab, U. Kammer, K. Hein and R. Rudert, *DD 236 348* (1986).
10. K. Hertwig, H. Bergmann and A. Rittel, *DE 4 210 917* (28 Jan. 1993).
11. H. Bergmann and A. Rittel, *Galvanotechnik* **92** (2001) 2664.
12. B. Delanghe, S. Tellier and M. Astruc, *Electrochim. Acta* **35** (1990) 1369.
13. N. Vatistas, P.F. Marconi and M. Bartolozzi, *Electrochim. Acta* **36** (1991) 339.
14. R. Carta, S. Palmas, A.M. Polcaro and G. Tola, *J. Appl. Electrochem.* **21** (1991) 793.
15. D.S. Lizárraga and J.M. Bisang, *J. Appl. Electrochem.* **26** (1996) 1209.
16. S. Langlois and F. Coeuret, *J. Appl. Electrochem.* **19** (1989) 51.
17. D. Pletcher, I. Whyte, F.C. Walsh and J.P. Millington, *J. Appl. Electrochem.* **21** (1991) 659.
18. A.T.S. Walker and A.A. Wragg, *Electrochim. Acta* **25** (1980) 323.
19. J.S. Newman and W. Tiedemann, *in* H. Gerischer and C.W. Tobias (Eds), 'Advances in Electrochemistry and Electrochemical Engineering', Vol. 11 (John Wiley & Sons, New York 1978), pp. 353–438.
20. M. Benzina, D. Mowla and Lacoste, *Chem. Eng. J.* **27** (1983) 1.
21. A. Karabelas and T. Wegner, *Chem. Eng. J.* **27** (1983) 1581.
22. D. Simonsson, *J. Appl. Electrochem.* **14** (1984) 595.
23. H. Olive and G. Lacoste, *Electrochim. Acta* **24** (1979) 1109.
24. R. Alkire, B. Gracon, T. Gruster, J. Marek and P. Blackburn, *J. Electrochem. Soc.* **127** (1980) 1085.
25. E.J. Wilson and C.J. Geankoplis, *Ind. Eng. Chem. Fund.* **5** (1966) 9.
26. I. Colquhoun-Lee and J. Stepanek, *Chem. Eng.* **282** (1974) 108.
27. G.A. Hughmark, *AIChE J.* **18** (1972) 1020.
28. F. Couret, *Electrochim. Acta* **21** (1976) 185.
29. H. Brauer and D. Mewes, *Chemie-Ing.-Techn.* **44** (1972) 93.
30. G. Kreysa, *Chemie-Ing.-Techn.* **55** (1983) 23.
31. R. Brandner, *PhD thesis*, University Dortmund (1982).
32. F. Nieber, *PhD thesis*, TH Köthen (1992).
33. D.A.G. Bruggemann, *Ann. Physik* **24** (1935) 636.
34. J.O'M. Bockris and J. Kim, *J. Appl. Electrochem.* **27** (1997) 890.
35. D.R. Lide, 'Handbook of Chemistry and Physics', 79th edition (CRC Press, New York 1998–99).
36. IMSL Numerical Library (1994).
37. R.H. Perry and C.H. Chilton, 'Chemical Engineers' Handbook' (McGraw-Hill, New York, 1973).
38. R.H. Perry and D.W. Green, 'Perry's Chemical Engineers' Handbook' (McGraw-Hill, New York, 1997).